

Surface Driven Bulk Reconstruction of Gold Nanorods

Yanting Wang,^a S. Teitel^a and Christoph Dellago^b

^a*Department of Physics and Astronomy, University of Rochester, Rochester, NY 14627*

^b*Institute for Experimental Physics, University of Vienna, Boltzmanngasse 5, 1090 Vienna, Austria*

Molecular dynamic simulations are used to study the heating of a gold nanorod of 2624 atoms. We show that roughening of surface $\{110\}$ facets leads to a shape transformation and structural rearrangement of surface and bulk atoms in the rod, in order to reach a more stable configuration. Our results show that the stability of the nanorod is governed by the free energetics of the surface facets.

PACS numbers: 64.70.Nd, 61.46.+w, 82.60.Qr

The properties of metallic clusters of various shapes, on the nanometer length scale, can be dramatically different from the corresponding bulk material due to their very large surface-to-volume ratio. The unique optical and mechanical properties of such nanoclusters hold great promise for the development of nanotechnology. Gold nanoclusters, for example, have found application in such diverse fields as nano-lithography [1], catalysis [2], nanobioelectronic devices [3], and ion detection [4]. It is therefore of great interest to study the behavior and stability of such nano-structures.

In this work we consider gold nanorods of low aspect ratio ~ 3 . Using molecular dynamic (MD) simulations of a rod with a few thousand atoms, we find that the stability of the nanorod upon heating is governed primarily by the energetics of its surface. When we start with a rod which has large $\{110\}$ surface facets, the roughening of these facets upon heating leads to a shape transformation of the rod to a shorter and wider structure. The surface reconstructs to form higher stability $\{111\}$ facets, while the fcc interior completely reorients to align with the new facet planes. When we start with a rod which has predominantly $\{111\}$ facets on its surface, the rod remains stable until melting.

The initial rod configuration that we consider, shown in Fig. 1, is one which has been proposed [5] to apply to recent experiments [6, 7, 8] on the laser heating of gold nanorods. The interior of the rod is a pure fcc lattice. The surface of the rod consists of four large $\{100\}$ and four large $\{110\}$ facets oriented parallel to the rod axis. The ends of the rod have a $\{001\}$ facet and four small $\{111\}$ facets connecting the $\{110\}$ and the $\{001\}$ facets. These experiments found that, upon heating, such rods underwent a shape transformation to bent, twisted, shorter, wider, and ϕ -shaped clusters. Transmission electron microscopy studies [8] observed point and planar internal defects to accompany such shape transformations. Recent MD simulations [9] of such rods, using a continuous heating procedure meant to model the laser heat-

ing of experiments, found similar shape transformations. These simulations found the shape transformation to be accompanied by a structural change in which planes of interior atoms shift, converting local fcc structure to hcp. The extent and stability of these interior rearrangements was found to depend upon both the heating rate and the number of atoms in the cluster, but no specific mechanism or energetic argument for this structural rearrangement was proposed. In this paper we present new simulations carried out with a much slower “quasi-equilibrium” heating that allows the rod more time to approach its lowest free energy configuration. Our results make it clear that it is the energetics of the surface that is driving the shape and structural transformation.

We use the empirical “glue” potential [10] to model the many body interactions of the gold atoms in our simulated nanorod, and we integrate the classical equations of motion for the atoms using the velocity Verlet algorithm [11] with a time step of 4.3 fs. However instead of increasing the kinetic energy at each MD step to model continuous heating as in Ref. [9], we now use the Gaussian isokinetic thermostat [12] to keep the total kinetic energy fixed at a constant temperature T ; after each MD step, all velocities are rescaled by a constant factor so as to keep $\langle (1/2)mv^2 \rangle = (3/2)k_B T$ fixed. Our procedure conserves total linear and angular momentum, which are set to zero, so that our rod does not drift or rotate throughout our simulation. At each fixed T we carry out 10^7 MD steps, for a simulated time of 43 ns, before increasing the temperature in jumps of 100 K. Our effective heating rate is therefore $\sim 2.3 \times 10^9$ K/s, more than three orders of magnitude slower than the continuous heating rates of $2-7 \times 10^{12}$ K/s used in Ref. [9]. We use a rod of $N = 2624$ atoms with initial aspect ratio of 3, as shown in Fig. 1. The length of the rod, parallel to its long axis, is 7.38 nm and its crosssectional area has a diameter of 2.46 nm. We do a short equilibration for 430 ps (10^5 MD steps) at 5 K in order to relax the surface atoms of the rod from their initial fcc positions, before starting to heat the rod.

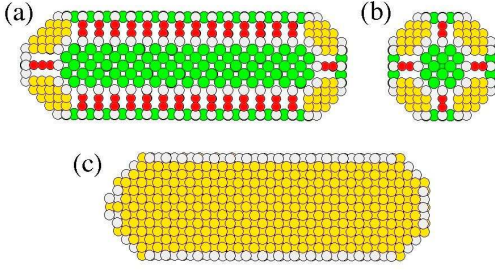


FIG. 1: Initial configuration of the gold nanorod with $N = 2624$ atoms and aspect ratio 3: (a) side view, (b) end view down the long axis, (c) cross-sectional view parallel to long axis. In (a) and (b), yellow atoms represent $\{111\}$ facets, green atoms $\{100\}$ facets, and red atoms $\{110\}$ facets; white atoms are on the edges. In (c), yellow atoms are those with a local fcc structure, white atoms are on the surface; the cross-sectional view in (c) shows atoms in the square arrangement of a $\{100\}$ plane of the fcc lattice.

As a signature of the shape change of our nanocluster we measure the radius of gyration, r_g , defined by $r_g^2 = (1/N) \sum_i |\mathbf{r}_i - \mathbf{r}_c|^2$, where \mathbf{r}_i is the position of atom i and \mathbf{r}_c is the center of mass. In Fig. 2a we plot our results for r_g as the system is heated; the blue curve is for our above “quasi-equilibrium” heating. The vertical dotted lines separate bins of constant temperature simulation, where the temperature is equal to the value at the left end point of the bin; the data plotted within each bin represents the instantaneous value of r_g as a function of increasing time at the constant temperature. At the end of each bin the temperature is increased by a jump of 100 K. We plot our data this way, instead of as an average value at each T , to highlight that significant shape relaxation occurs even at constant T . For comparison, we plot r_g for the continuous heating (red curve) of Ref. [9] for the heating rate of 7×10^{12} K/s. We see that the curves are qualitatively similar, with the onset of a plateau around 800 K, however the present quasi-equilibrium heating allows the rod to relax to smaller r_g values, before the rod melts at $T \sim 1200$ K. The decrease in the radius of gyration reflects the shape transformation to a shorter wider rod of smaller aspect ratio.

To investigate the local structure within the cluster, we use the method of bond orientational order parameters [13]. These parameters measure the orientation of bonds connecting a given atom to its nearest neighbors, and provide a convenient means of determining the local crystalline structure of an atom. In particular, we measure the 6-fold and 4-fold orientation parameters, Q_6 , \hat{W}_6 , Q_4 , and \hat{W}_4 . We refer the reader to the literature for their definitions [9, 13], and in Table I we give their values for several periodic three dimensional crystal structures. We also, in Table I, give the values of these parameters as computed for atoms on particular low index planar surfaces of an fcc bulk crystal; for these two dimensional pa-

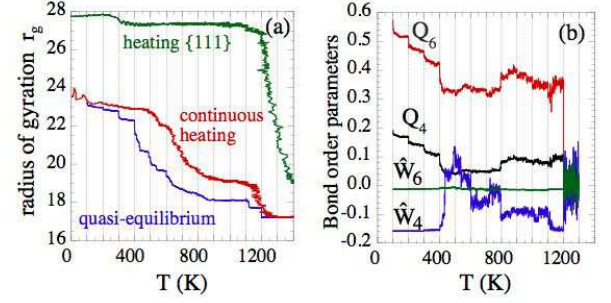


FIG. 2: (a) Radius of gyration r_g vs. temperature T for the rod of Fig. 1: quasi-equilibrium heating (blue) compared to the continuous heating of Ref. [9] (red); continuous heating of the rod with structure of Fig. 3 (green). (b) Bond order parameters, Q_4 , Q_6 , \hat{W}_4 and \hat{W}_6 , averaged over all atoms internal to the rod, vs. temperature T , for quasi-equilibrium heating of the rod of Fig. 1.

TABLE I: Bond order parameters for face-centered-cubic (fcc), hexagonal close-packed (hcp), simple cubic (sc), body-centered-cubic (bcc), and low index fcc planes.

Geometry	Q_4	Q_6	\hat{W}_4	\hat{W}_6
fcc	0.190 94	0.574 52	-0.159 32	-0.013 16
hcp	0.097 22	0.484 76	0.134 10	-0.012 44
sc	0.763 76	0.353 55	0.159 32	0.013 16
bcc	0.082 02	0.500 83	0.159 32	0.013 16
$\{110\}$	1	1	0.134 10	-0.093 06
$\{100\}$	0.829 16	0.586 30	0.124 97	-0.007 21
$\{111\}$	0.375 00	0.740 83	0.134 10	-0.046 26

rameters we average only over bonds connecting an atom with its neighbors in the specified plane. In Fig. 2b we plot these order parameters for our rod, averaging over only atoms internal to the rod (i.e. we exclude surface atoms since these have fewer nearest neighbor bonds). As for r_g , we plot our data as the instantaneous value as a function of increasing simulation time, for bins of constant temperature (indicated by the dotted vertical lines).

Comparing with Table I, we see that the rod maintains its fcc structure until about 400 K. Then, from around 400 K to about 800 K, there is a rise to positive values in \hat{W}_4 , and a decrease in Q_6 and \hat{W}_6 , suggestive of a more hcp-like structure. Above 800 K, the values return to their fcc-like values.

We now focus on the structure of the rod in the high temperature plateau region where r_g stabilizes to a constant. In Fig. 3 we show the configuration of the rod at $T = 900$ K, in the constant plateau region before melting. The views of the rod shown in Figs. 3a,b,c are the same orientations as shown for the initial configuration in Figs. 1a,b,c. In order to better illustrate the order of the rod, we first pick an instantaneous configuration

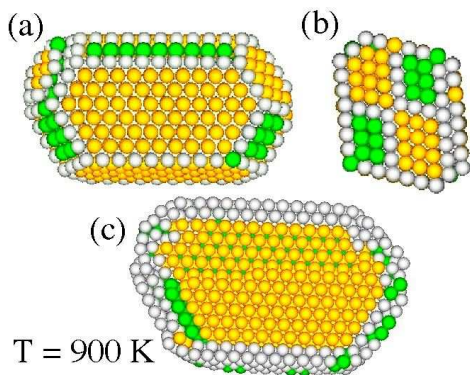


FIG. 3: Configuration of the nanorod after quasi-equilibrium heating to 900 K. (a) side view, and (b) end view down the long axis, after peeling away the surface and the first sub-surface layer; yellow atoms are $\{111\}$ facets, green atoms are $\{100\}$ facets, and white are edge atoms. (c) cross-sectional view parallel to the long axis; yellow atoms have a local fcc structure, green atoms have a local hcp structure, and white atoms are neither. The cross-sectional view in (c) shows atoms in the close-packed hexagonal arrangement of a $\{111\}$ plane of the fcc lattice.

sampled from the middle of the $T = 900 \text{ K}$ simulation, and use the conjugate gradient method [14] to quench local thermal fluctuations. At such high temperatures, the surface can be partially disordered compared to the interior, due to the diffusion of atoms on and near facet edges and vertices [15, 16]. We therefore use the *cone algorithm* [16] to identify and peel away atoms on the surface and in the first sub layer below it, and in Figs. 3a,b show the configuration of the second sub layer of the rod. We see a very regular shape covered almost completely with stable $\{111\}$ facets. Based on the values in Table I, we use the following criteria to identify atoms in this layer as belonging to particular low index planes: $\{111\}$ if $0.7 < Q_6 < 0.9$ and $-0.08 < \hat{W}_6 < -0.02$; $\{100\}$ if $Q_6 < 0.7$ and $\hat{W}_6 > -0.02$; and $\{110\}$ if $Q_6 > 0.9$ and $\hat{W}_6 < -0.08$. Atoms in Figs. 3a,b have been colored accordingly.

The cross-sectional view in Fig. 3c shows an almost pure fcc interior, as was the case for the initial configuration, however we now see a close packed hexagonal structure characteristic of a $\{111\}$ plane of the fcc lattice, rather than the $\{100\}$ plane seen in the cross-sectional view of Fig. 1c. We thus see one of our main results: in order to align with the new $\{111\}$ surface facets, the bulk fcc structure has completely reconstructed itself to a new orientation. For interior atoms, we use the following criteria to identify the local crystal structure: fcc if $Q_4 > 0.17$ and $\hat{W}_4 < -0.10$; hcp if $Q_4 < 0.13$ and $\hat{W}_4 > 0.07$. Atoms in Figs. 3c have been colored accordingly.

To see how the rod evolves from its initial configuration (Fig. 1) to its reconstructed shape (Fig. 3), we consider

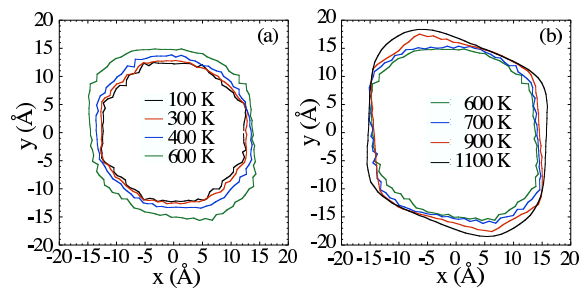


FIG. 4: Average cross-sectional shape, viewed down the long axis of the rod, for different temperatures.

the average cross-sectional shape in a plane transverse to the long axis of the rod. We compute this average shape as follows. For each instantaneous configuration we first eliminate all atoms on the end caps of the rods, and all interior atoms of the rod, and then project the remaining surface atoms into the xy plane, perpendicular to the long axis of the rod. Placing the origin at the resulting center of mass, we divide the plane into 100 equal polar angles, and then compute the average position of all surface atoms in each angular division. This result is then averaged over 1000 different instantaneous configurations sampled uniformly throughout the simulated time of 43 ns at each temperature T . We plot the resulting average cross-sectional shapes, for several different T , in Fig. 4.

At low T we see the octagonal cross-section of the initially constructed rod of Fig. 1, with the flat edges representing the initial $\{100\}$ and $\{110\}$ facets. The shape stays roughly the same until about 400 K. Somewhere between 300 – 400 K, the shape becomes rounder and the initial flat edges disappear. As T increases further, the cross-sectional area grows, representing the shape transformation to a shorter and wider rod of lower aspect ratio, and we see new flat facets develop and grow in new directions. At 900 K we see the fully faceted shape shown in Fig. 3.

The disappearance of the initial flat facets, with the resulting rounding of the average shape, is a signature of the roughening transition of those surfaces [17]. For *macroscopic* gold samples, it is known from experiments that the $\{110\}$ surface roughens at 680 K [18], while the $\{100\}$ surface disorders at $\sim 1170 \text{ K}$ [19], below the bulk melting temperature of 1337 K. In contrast, the $\{111\}$ surface is believed to remain stable up to, and even above, the bulk melting [20]. The initiation of the shape change that we find in our nanorod at 400 K is most likely a consequence of the roughening transition of the $\{110\}$ facets, which has been shifted to lower temperature due to large finite size effects in our relatively small rod (just as the bulk melting transition can be greatly reduced by finite size effects [21]). After this roughening, the surface reconstructs to form mostly lower free energy $\{111\}$ facets, which remain stable until melting. Note that the fully

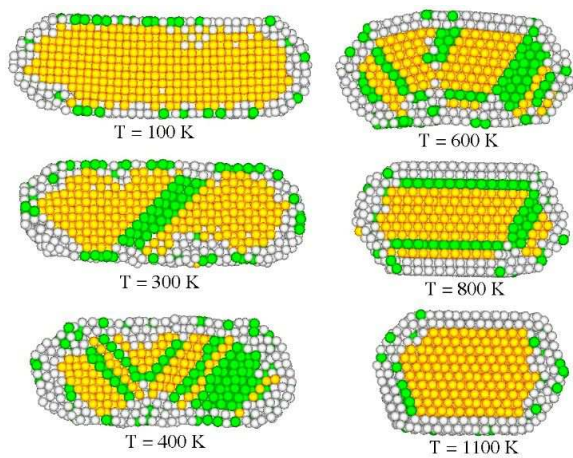


FIG. 5: Cross-sectional view for various temperatures. Atoms are colored according to local crystal structure: fcc is yellow, hcp is green, neither is white.

faceted cross-sectional shape at 900 K contains four large sides and two short sides; the former are the $\{111\}$ facets, while the latter are $\{100\}$ facets. By 1100 K, these $\{100\}$ facets have been replaced by a smoothly curved surface. We infer that this is due to the disordering transition of the $\{100\}$ surface, reduced somewhat in temperature due to finite size effects.

In order to see how the interior fcc structure of the rod reconstructs itself to a new orientation, we show in Fig. 5 cross-sectional views of the rod at various temperatures. We color the atoms according to their local crystal structure, using the criteria given above: fcc is yellow, hcp is green, neither is white. Initially, the interior is pure fcc, oriented so that the cross-sectional view shows a $\{100\}$ plane of atoms. As temperature increases, we see that the shape and structural transformation is accompanied by the appearance of hcp planes inside the rod interior, due to the sliding of $\{111\}$ planes. As temperature further increases, the surface becomes less ordered, and more $\{111\}$ planes with different orientation slide. Around 800 K, the surface has reordered and the interior fcc lattice has reoriented so that the cross-sectional view now shows a predominantly $\{111\}$ plane of atoms. At 1100 K, the interior has completely reordered to pure fcc, but with the new orientation.

Such behavior as described above may well exist in other simple elemental metals. We note that many such metals similarly have a roughening transition T_R for the $\{110\}$ surface that is significantly below the bulk melting T_m . Silver, for example, has $T_R = 600$ K and $T_m = 1235$ K, with a similar ratio of T_R/T_m as gold [22]. Lead has $T_R = 415$ K and $T_m = 601$ K, for a somewhat larger T_R/T_m than gold [23].

Finally, in order to verify that the roughening of the $\{110\}$ facets, rather than just the minimization of total surface area, is indeed the mechanism for the shape trans-

formation, we study the stability of a gold nanorod with an aspect ratio of ~ 3 , but with an initial structure similar to that of Fig. 3, with a surface predominantly covered by $\{111\}$ facets. We use a continuous heating MD simulation with a heating rate of 7×10^{12} K/s to model laser heating experiments, for a rod with 3411 atoms. Our results for r_g vs T are shown in Fig. 2a (green curve). Unlike the initial rod of Fig. 1, we now find that the rod remains stable, with no significant shape or structural rearrangement, up until the rod melting temperature. We conclude that the stability of gold, and presumably other metallic, nanorods is crucially dependent upon the structure of the rod surface.

This work was funded in part by DOE grant DE-FG02-89ER14017.

-
- [1] J. Zheng, Z. Chen, and Z. Liu, *Langmuir* **16**, 9673 (2000).
 - [2] A. T. Bell, *Science* **299**, 1688 (2003).
 - [3] Y. Xiao, F. Patolsky, E. Katz, J. F. Hainfeld, and I. Willner, *Science* **299**, 1877 (2003).
 - [4] S. O. Obare, R. E. Hollowell, and C. J. Murphy, *Langmuir* **18**, 10 407 (2002).
 - [5] Z. L. Wang, M. B. Mohamed, S. Link and M. A. El-Sayed, *Surf. Sci* **440**, L809 (1999).
 - [6] S. Chang, C. Shih, W. Lai and C. R. C. Wang, *Langmuir* **103**, 1165 (1999).
 - [7] S. Link, C. Burda, B. Nikoobakht and M. A. El-Sayed, *J. Phys. Chem B* **104**, 6152 (2000).
 - [8] S. Link, Z. L. Wang and M. A. El-Sayed, *J. Phys. Chem B* **104**, 7867 (2000).
 - [9] Y. Wang and C. Dellago, *J. Phys. Chem. B* **107**, 9214 (2003).
 - [10] F. Ercolessi, M. Parrinello and E. Tosatti, *Philos. Mag. A* **58**, 213 (1988).
 - [11] M. P. Allen, D. J. Tildesley, *Computer Simulation of Liquids* (Clarendon Press, Oxford, 1987).
 - [12] D. J. Evans, W. G. Hoover, B. H. Failor, B. Moran and A. J. C. Ladd, *Phys. Rev. A* **28**, 1016 (1983).
 - [13] P. J. Steinhardt, D. R. Nelson and M. Ronchetti, *Phys. Rev. B* **28**, 784 (1983).
 - [14] W. H. Press, S. A. Teukolsky, W. T. Vetterling and B. P. Flannery, *Numerical Recipes in C: The Art of Scientific Computing* (Cambridge University Press, Cambridge, 1992).
 - [15] Y. Wang, S. Teitel and C. Dellago, *Chem. Phys. Lett.* **394**, 257 (2004).
 - [16] Y. Wang, S. Teitel and C. Dellago, cond-mat/0408458.
 - [17] C. Jayaprakash, W. F. Saam and S. Teitel, *Phys. Rev. Lett.* **50**, 2017 (1983).
 - [18] A. Hoss, M. Nold, P. von Blanckenhagen and O. Meyer, *Phys. Rev. B* **45**, 8714 (1992).
 - [19] B. M. Ocko, D. Gibbs, K. G. Huang, D. M. Zehner and S. G. J. Mochrie, *Phys. Rev. B* **44**, 6429 (1991); S. G. J. Mochrie, D. M. Zehner, B. M. Ocko and D. Gibbs, *Phys. Rev. Lett.* **64**, 2925 (1990).
 - [20] K. G. Huang, D. Gibbs, D. M. Zehner, A. R. Sandy and S. G. J. Mochrie, *Phys. Rev. Lett.* **65**, 3313 (1990); G. M. Watson, D. Gibbs, S. Song, A. R. Sandy, S. G. J. Mochrie

- and D. M. Zehner, Phys. Rev. B **52**, 12329 (1995); P. Carnevali, F. Ercolessi and E. Tosatti, Phys. Rev. B **36**, 6701 (1987).
- [21] Ph. Buffat and J.-P. Borel, Phys. Rev. A **13**, 2287 (1976).
- [22] L. Pedemonte and G. Bracco, Surf. Sci. **513** 308, (2002).
- [23] H.-N. Yang, T.-M. Lu, and G.-C. Wang, Phys. Rev. Lett. **63**, 1621 (1989).